2011

Flt3L controls the development of radiosensitive dendritic cells in the meninges and choroid plexus of the steady-state mouse brain

Niroshana Anandasabapathy

Gabriel D. Victora

Matthew M. Meredith

Flt3L controls the development of radiosensitive dendritic cells in the meninges and choroid plexus of the steady-state mouse brain

Niroshana Anandasabapathy,[1,2] Gabriel D. Victora,[3,5,6] Matthew Meredith,[3] Rachel Feder,[1,2] Baojun Dong,[7] Courtney Kluger,[1,2] Kaihui Yao,[3] Michael L. Dustin,[5,6] Michel C. Nussenzweig,[3,4] Ralph M. Steinman,[1,2] and Kang Liu[3,7]

[1]Laboratory of Cellular Physiology and Immunology, [2]Christopher H. Browne Center for Immunology and Immune Diseases, [3]Laboratory of Molecular Immunology, and [4]Howard Hughes Medical Institute, The Rockefeller University, New York, NY 10065
[5]Helen L. and Martin S. Kimmel Center for Biology and Medicine, Skirball Institute of Biomolecular Medicine and [6]Department of Pathology, New York University School of Medicine, New York, NY 10016
[7]Department of Microbiology and Immunology, Columbia University Medical Center, New York, NY 10032

Antigen-presenting cells in the disease-free brain have been identified primarily by expression of antigens such as CD11b, CD11c, and MHC II, which can be shared by dendritic cells (DCs), microglia, and monocytes. In this study, starting with the criterion of Flt3 (FMS-like receptor tyrosine kinase 3)-dependent development, we characterize the features of authentic DCs within the meninges and choroid plexus in healthy mouse brains. Analyses of morphology, gene expression, and antigen-presenting function established a close relationship between meningeal and choroid plexus DCs (m/chDCs) and spleen DCs. DCs in both sites shared an intrinsic requirement for Flt3 ligand. Microarrays revealed differences in expression of transcripts encoding surface molecules, transcription factors, pattern recognition receptors, and other genes in m/chDCs compared with monocytes and microglia. Migrating pre-DC progenitors from bone marrow gave rise to m/chDCs that had a 5–7-d half-life. In contrast to microglia, DCs actively present self-antigens and stimulate T cells. Therefore, the meninges and choroid plexus of a steady-state brain contain DCs that derive from local precursors and exhibit a differentiation and antigen-presenting program similar to spleen DCs and distinct from microglia.

CORRESPONDENCE
Kang Liu:
kl2529@columbia.edu

Abbreviations used: cDC, conventional DC; CDP, common DC progenitor; CNS, central nervous system; Flt3L, Flt3 ligand; m/chDC, meningeal and choroid plexus DC; MDP, monocyte and DC progenitor; MOG, myelin oligodendroglial glycoprotein; mRNA, messenger RNA.

The steady-state brain is associated with immune privilege, i.e., a paucity of lymphocytes and an inability to initiate immunity. The latter has been attributed, at least in part, to a lack of DCs (Bailey et al., 2006). Central nervous system (CNS) infiltration of leukocytes has been largely perceived as a feature of neuroinflammation in which there is a break in the blood brain barrier (Hickey, 1991; Platten and Steinman, 2005; Bailey et al., 2007).

In spite of immune privilege, an immune contribution to hippocampal neurogenesis was first proposed based on the observation that T cell loss is associated with dementia arising in both HIV patients and recipients of immunosuppressive chemotherapy (Price et al., 1988; Hess and Insel, 2007). Improved cognitive function occurs during reconstitution of T cell immunity in both humans and mice (Ziv et al., 2006; Kipnis et al., 2008; Wolf et al., 2009). Recent studies demonstrate that in the healthy CNS, memory and cognition are $CD4^+$ T cell dependent. In particular, IL-4–producing T cells accumulate in the meningeal space during cognitive tasks (Derecki et al., 2010). That learning is impaired in the absence of $CD4^+$ T cell cytokine production links, for the first

The Rockefeller University Press $30.00
J. Exp. Med. Vol. 208 No. 8 1695-1705
www.jem.org/cgi/doi/10.1084/jem.20102657

time, immune activity to steady-state cognitive function. The meninges and the choroid plexus were also recently demonstrated to be the site or gateway for entry of activated effector T cells into the CNS (Axtell and Steinman, 2009; Bartholomäus et al., 2009; Reboldi et al., 2009). These findings leave a major gap: what is the nature of the APCs that guide T cell function?

DCs are specialized APCs that mediate systemic T cell tolerance and immunity (Banchereau and Steinman, 1998; Heath and Carbone, 2009). In the steady-state, most DCs originate from a common DC precursor called pre-DCs (Liu et al., 2009). Pre-DCs arise from committed DC progenitors in the bone marrow, migrate through the blood, and seed lymphoid and nonlymphoid tissues, where they undergo a limited number of divisions and differentiate into specialized DC subsets (Liu et al., 2009). DC development is dependent on Flt3 (FMS-like receptor tyrosine kinase 3) ligand (Flt3L), a hematopoietin acting primarily on DCs and their progenitors that express Flt3/CD135 receptor, both in the bone marrow and the periphery (Waskow et al., 2008; Kingston et al., 2009).

Resident DCs have been defined in nonlymphoid organs including the skin, lung, gut, and kidney (Bogunovic et al., 2009; Ginhoux et al., 2009; Rescigno and Di Sabatino, 2009; Varol et al., 2009; Henri et al., 2010), but there is little characterization of DCs in the steady-state brain. The choroid plexus and meninges were identified as the gates of entry for activated T cells into the brain by a mechanism involving the chemokine receptor CCR6 (Kivisäkk et al., 2003; McMenamin et al., 2003; Bartholomäus et al., 2009; Reboldi et al., 2009). Cell surface staining with individual markers MHC II, CD11c, CD11b, OX62, and DEC205 suggested the presence of APCs in the choroid plexus and meninges, and functional study of targeted MHC II expression in $CD11c^+$ cells attributed the onset of neuroinflammation to an increase of APCs in these gateways (Matyszak and Perry, 1996; McMenamin, 1999; Greter et al., 2005; Serafini et al., 2006; Kivisäkk et al., 2009). However, a precise characterization of these APCs in the steady-state is lacking because of their limited numbers, a lack of imaging tools, and the absence of lineage-specific markers. Also, as discussed extensively elsewhere (Geissmann et al., 2010), the aforementioned markers MHC II, CD11c, CD11b, and DEC205 lack specificity and as such fail to differentiate among multiple lineages. Identification of the DC lineage requires information on location, development, transcriptional programs, and function.

High levels of CD11c, for instance, was initially identified as a useful marker to identify DCs, and the CD11c promoter was used to generate genetically modified mice to study DC distribution and function. Indeed, studies with CD11c-DTR and CD11c-DT as well as CD11c-MHC II mice demonstrated that DCs could both prime T cells and maintain T cell tolerance, but these studies include complementary experiments with isolated DCs, typically from lymphoid tissues (Jung et al., 2002; Lemos et al., 2003). However, CD11c is not restricted to conventional DC (cDC) lineage as the expression is also found on monocytes, plasmacytoid DCs, activated lymphocytes, and activated microglia (Geissmann et al., 2003; Gottfried-Blackmore et al., 2009). CD11b, commonly used as the macrophage marker, also lacks lineage specificity and is expressed by macrophages, monocytes, microglia, and some DC subsets (Geissmann et al., 2010). In this study, to better identify and understand APCs in the steady-state brain, we used developmental criteria, transcriptional profiling, and function and used these components of cell function to distinguish DCs from monocytes, macrophages, and microglia.

RESULTS

Flt3L selectively expands CD11c and MHC II–high leukocytes in the disease-free mouse brain

To identify DCs in the steady-state brain, we phenotyped $CD45^+$ leukocytes in cell suspensions, comparing normal mice with those treated with Flt3L, a potent DC hematopoietin. Based on the responsiveness of the DC lineage to Flt3L in many tissues, we reasoned that this hematopoietin might expand and better define populations of brain DCs. Additionally, we revisited previously described CD11c–enhanced YFP (EYFP) reporter mice to detect EYFP-high DCs with a characteristic morphology (Lindquist et al., 2004; Choi et al., 2009). In naive CD11c-EYFP mice, flow cytometry analysis for EYFP and CD45 expression (to identify leukocytes) showed $EYFP^+$ cells in both $CD45^{int}$ and $CD45^{hi}$ populations, but 14 d after Flt3L treatment, only the $CD45^{hi}EYFP^+$ cells expanded and expressed high cell surface CD11c and MHC II (Fig. 1 A). In contrast, $CD45^{int}EYFP^+$ and $EYFP^-$ cells did not expand with Flt3L treatment. The nonresponsive $CD45^{int}EYFP^+$ cells were CD11c and MHC II negative in contrast to the responsive $CD45^{hi}EYFP^+CD11c^+$MHC II^+ cells (Fig. 1 A). Interestingly, CD11c-EYFP mouse spleen also contains two populations of $EYFP^+$ cells. One population with a $CD11c^+$MHC II^+ cDC phenotype expanded in response to Flt3L injection. In contrast, the other $CD11c^{lo}$ population, the majority of which displayed a $CD11b^{lo}F4/80^{hi}$ red-pulp macrophage phenotype, did not respond to Flt3L injection (Fig. 1 B). Thus, we conclude that CD11c-EYFP mouse spleen and brain contain two populations of $EYFP^+$ cells that are developmentally distinct based on their Flt3L responsiveness.

In the brains of nontransgenic C57BL/6 (B6) mice, i.e., without the use of the CD11c-EYFP reporter, a population of $Lin^-CD45^{hi}CD11c^{hi}$MHC II^{hi} cells was detected, and these were the cells that expanded more than fivefold after Flt3L treatment (Fig. 1, C and D). In contrast, $Lin^-CD45^{int}CD11c^-$ cells, presumably microglia, did not show significant responses to Flt3L treatment (Fig. 1, C and D). These data with Flt3L responsiveness and CD11c/MHC II expression strongly imply the presence of cells in the brain that are similar to DCs in other organs.

Flt3L-responsive DCs localize to the meninges and choroid plexus

To localize these populations in naive and Flt3L-treated mice, we examined brains from CD11c-EYFP transgenic

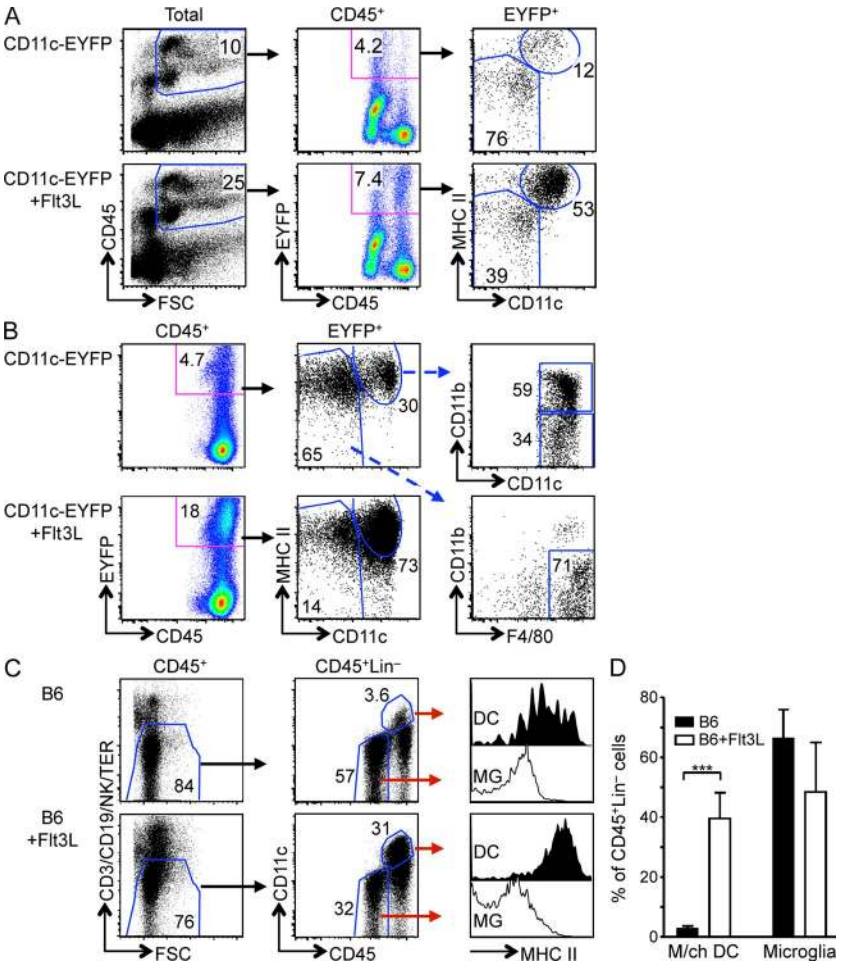

Figure 1. Phenotype of Flt3L-responsive CD45^{hi}CD11c^{+}MHC II^{+} cells in the steady-state mouse brain. (A and B) Flow cytometric dot plots of EYFP expression in brain leukocytes (A) and the splenocytes (B) of untreated (top) versus Flt3L-treated (bottom) CD11c-EYFP transgenic mice. Numbers indicate percentage of gated cells. Data are representative of three independent experiments. (C) Flow cytometric dot plots of CD45^{+} mononuclear cells in the brain of untreated (top) versus Flt3L-treated (bottom) nontransgenic C57BL/6 mice. Histograms show MHC II staining on the surface of DCs and microglia (MG) from the indicated gates. Data are representative of more than three independent experiments. (D) Bar graph shows quantification of m/chDCs and microglia 14 d after Flt3L treatment in B6 mice. Bars represent data from two pooled experiments, each with two brains. Error bars represent the mean ± SEM (n = 4; ***, P < 0.0001).

mice with two-photon microscopy. We detected EYFP^{+} cells along the meninges, in the choroid plexus, and in the parenchyma of coronal sections (Fig. 2 A). We then labeled blood vessels with DiI dye and imaged the intact brain en face, from the top downward. DiI labeled major blood vessels in the dura mater (Fig. 2 B, top) as well as capillary blood vessels in the pia mater (Fig. 2 B, bottom), marking the anatomical layers of the meninges. Some but not all EYFP^{+} cells with thick dendrites were located near meningeal blood vessels (Fig. 2 B). After Flt3L treatment, a dramatic expansion of EYFP^{+} cells was observed in discrete patches along the meninges, but in contrast, no significant change in the quantity of parenchymal EYFP^{+} cells was observed (Fig. 2 C). EYFP^{+} cells in the meninges and choroid plexus displayed a distinct morphology, with large cell bodies and several thick dendrites per cell, which is consistent with that of typical DCs. In contrast, parenchymal EYFP^{+} cells were highly ramified and displayed a phenotype typical of microglia (Fig. 2 A, bottom).

Next, we compared bulk meninges and parenchyma to meningeal isolates in the presence and absence of Flt3L treatment. Consistent with the localization of EYFP^{+} cells in the meninges of CD11c reporter mice by microscopy, flow cytometric analysis showed that most meningeal and splenic EYFP^{+} cells were CD11c^{+}MHC II^{+}; in contrast, the majority of EYFP^{+} cells in brain parenchyma displayed a microglia phenotype, i.e., CD45^{int}CD11c^{-} MHC II^{-} (Fig. S1). In line with the data from CD11c-EYFP reporter mice, we observed an enrichment of CD11c^{+}CD45^{hi} DCs in the meninx preparations from naive B6 WT animals (7.5% ± 0.35%) when compared with whole brain preparations (3 ± 0.66%) of untreated mice (Fig. 2 D). A marked enrichment in DC numbers was quantified by flow cytometry in the meningeal preparation and in whole brain preps after Flt3L treatment, whereas microglia numbers remained unchanged in whole brain (Fig. 2 D, graph). We also examined the meninges from CX$_3$CR1$^{gfp/+}$ mice. In contrast to microglia that were mostly CX$_3$CR1-GFP^{+} (95%), meningeal DCs and spleen DCs were heterogeneous in CX$_3$CR1-GFP (Fig. S2 A), and both CX$_3$CR1-GFP^{+} and CX$_3$CR1-GFP^{-} DCs were expanded by Flt3L (Fig. S2 B).

For further confirmation, we examined I-A^{b}–EGFP knockin mice, in which cellular MHC II levels correlate with EGFP signal (Boes et al., 2002). En face two-photon imaging revealed numerous EGFP^{+} cells with classical DC morphology in the upper 30 µm of the brain, corresponding to the dura mater and pia mater of the meninges. In contrast, no EGFP^{+} cells were detected deeper in the tissue (35–90 µm), which correlated with the parenchyma immediately below the meninges (Fig. 2 E and Video 1). Coronal sectioning likewise revealed EGFP^{+} cells with DC morphology in the choroid plexus but not in the parenchyma in the steady-state (Fig. 2 E). Flow cytometry confirmed that all Lin^{-}CD45^{hi}CD11c^{+} but none of the Lin^{-}CD45^{int}CD11c^{-} brain leukocytes in these mice were EGFP^{+} (Fig. 2 E). Therefore, the data from I-A^{b}–EGFP mice again indicate the

presence of MHC II$^+$ cells with DC morphology in the meninges and choroids plexus but not in the parenchyma of the mouse brain.

These observations show that the Lin$^-$CD45^{hi}CD11c$^+$ MHC II$^+$ brain cells correspond to Flt3L-responsive EYFP cells with typical DC morphology, and they are located in the meninges and choroid plexus. We will refer to CD45/CD11c/MHC II^{hi} cells in the brain as meningeal and choroid plexus DCs (m/chDCs), as opposed to microglia, which are Lin$^-$CD45^{int}CD11c$^{-/lo}$MHC II$^-$.

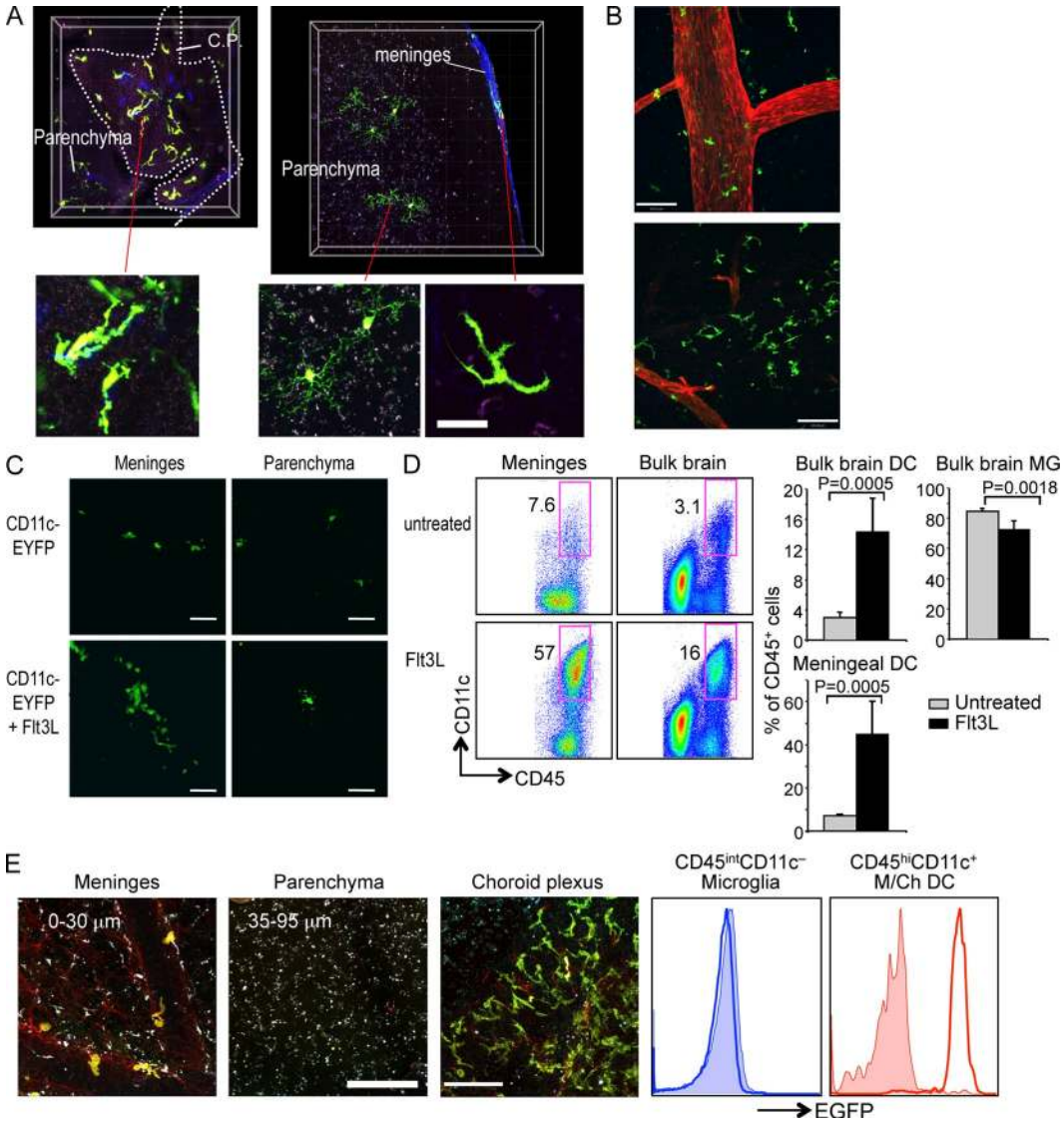

Figure 2. Flt3L-responsive cells with dendritic morphology within meninges and choroid plexus. (A) Two-photon microscopy showing fluorescent cells in coronal brain sections of untreated CD11c-EYFP mice. EYFP$^+$ cells were detected in choroid plexus (C.P.) and parenchyma (top left) and meninges and parenchyma (top right). Small panels at the bottom show the morphology of individual EYFP$^+$ cells from choroid plexus, meninges (en face view), and parenchyma. (B) En face two-photon view of the brains of untreated CD11c-EYFP mouse brains. Blood vessels (red) were labeled by perfusion with DiI. EYFP$^+$ (green) cells were detected in the meninges. Panels show a major blood vessel in the dura mater (top) and capillary blood vessels in the pia mater (bottom). (C) Two-photon microscopy coronal sections from the brain of untreated (top) and Flt3L-treated (bottom) CD11c-EYFP mice (green, EYFP). (D) Flow cytometric analysis of DCs in meningeal isolates. Dot plots show gated CD45^{hi}CD11c^{hi} DCs in CD45$^+$ leukocytes of meningeal isolates and whole brain preparation in untreated or Flt3-treated B6 mice. Numbers indicate percentage of each cell type within total CD45$^+$ cells. Bar graphs summarize the percentage of m/chDCs and microglia (MG) among CD45$^+$ brain leukocytes in untreated versus Flt3L-treated mice in bulk brain and meninges (gating shown in Fig. S1 B). Bars show data from one representative experiment (n = 5 mice per group). Error bars represent the mean ± SD (n = 5). (E) Two-photon microscopy and flow cytometry of EGFP$^+$ cells in the brain of I-A^b–EGFP transgenic mice. (microscopy) Observation in meninges 0–30 µm (left) and parenchyma 35–90 µm (middle) from the upper limit of the brain and in choroid plexus (right) from coronal sections of untreated I-A^b–EGFP mice (yellow, EGFP; red, collagen fiber; white, autofluorescence). Flow cytometry histograms show overlay of EGFP expression on microglia and m/chDCs, gated as in Fig. 1 B, from WT B6 (shaded area) and I-A^b–EGFP (line) mice. Data are representative of two independent experiments. Bars: (A, C, and E) 50 µm; (B) 100 µm.

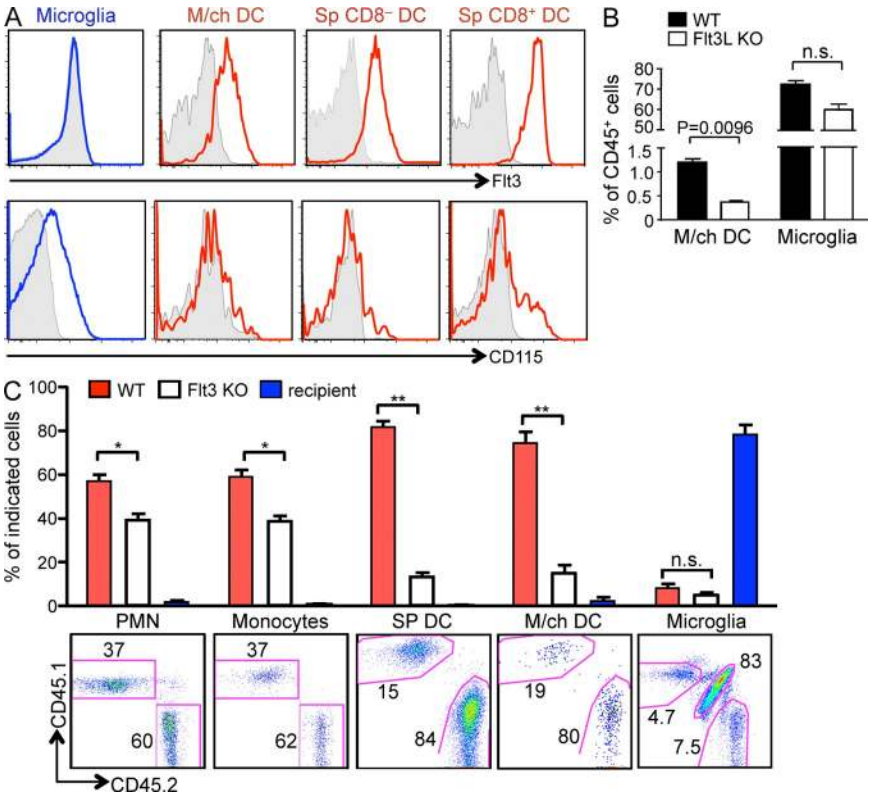

Figure 3. m/chDCs express Flt3 and have an intrinsic dependence on Flt3L. (A) Histograms show cell surface expression of Flt3 receptor and M-CSF receptor (CD115; line) or isotype antibody control (shaded area) on gated microglia and m/chDCs in the brain versus CD8$^-$ and CD8$^+$ DC subsets in the spleen (Sp). (B) Bar graph shows percentage of m/chDCs and microglia among CD45$^+$ brain leukocytes in WT versus Flt3L KO mice. Bars represent data from two pooled experiments ($n = 4$). Error bars represent the mean ± SEM ($n = 4$). (C) Lethally irradiated CD45.1$^+$CD45.2$^+$ F1 recipient mice were reconstituted with a mixture of 50% CD45.1$^+$ Flt3 KO and 50% CD45.2$^+$ WT bone marrow and analyzed 2–3 mo later. Bar graph shows the percentage of indicated cells from Flt3 KO CD45.1$^+$ (open) and WT CD45.2$^+$ (red) donor or CD45.1$^+$CD45.2$^+$ recipient (blue) origin. Bars represent data from three animals. Error bars represent the mean ± SEM ($n = 3$; *, $P < 0.05$; **, $P < 0.01$). Dot plots show percentage of donor and recipient cells in gated cell populations analyzed by flow cytometry, representing two independent experiments.

et al., 2007). We conclude that brain m/chDCs, in contrast to microglia, are radiosensitive and that their development is dependent on Flt3 signaling.

m/chDCs express Flt3 and have an intrinsic requirement for Flt3 signaling

To understand the development of m/chDCs, we pursued findings that classical DCs in lymphoid and other nonlymphoid organs, such as liver, gut, kidney, and lung, express Flt3 (or Flk2) and that their development critically depends on Flt3 signaling (Bogunovic et al., 2009; Ginhoux et al., 2009). Similar to spleen DCs, m/chDCs expressed cell surface Flt3/CD135 but not M-CSFR/CD115, whereas microglia were Flt3 negative and M-CSFR positive (Fig. 3 A). Likewise, in Flt3L KO mice, we observed an 80% decrease in the number of m/chDCs, whereas microglia developed normally (Fig. 3 B).

To determine whether the requirement for Flt3 signaling was intrinsic to m/chDCs, we made mixed bone marrow chimeras in which 50:50 mixtures of marrow from Flt3$^{+/+}$ CD45.2 and Flt3$^{-/-}$ CD45.1 mice were injected into lethally irradiated CD45.1 × CD45.2 F1 recipients. Because neutrophil development is independent of Flt3, their representation from each donor was used to follow the input ratio of hematopoietic stem cells in each mouse. As a positive control, we found that Flt3$^{-/-}$ spleen DCs were outcompeted by Flt3$^{+/+}$ DCs, whereas splenic monocytes, which are Flt3 independent, arose from Flt3$^{+/+}$ and Flt3$^{-/-}$ stem cells in ratios equal to the neutrophil ratios (Fig. 3 C). Brain m/chDC development was similar to that of spleen DCs, demonstrating an intrinsic requirement for Flt3 signaling (Fig. 3 C). However, microglia were largely radio resistant and retained the host phenotype (Fig. 3 C), as expected from prior research (Mildner

m/chDCs and CD8$^+$ spleen DCs share gene expression profiles

To further understand the functional relationship between m/chDCs and other myeloid cells, we compared the gene expression profile of m/chDCs with that of bone marrow monocytes, brain microglia, and classical spleen CD8$^+$ and CD8$^-$ DCs. To obtain enough m/chDCs for messenger RNA (mRNA) extraction, we expanded m/chDCs with in vivo Flt3L treatment before purification. Consistent with a previous study showing that Flt3L stimulates DC expansion without maturing them (Dudziak et al., 2007), we found no change in maturation markers CD80, CD86, CD40, and MHC II (I-A) in Flt3L-treated m/chDCs (Fig. S3). With respect to growth factor receptors, m/chDCs expressed high levels of Flt3 and low levels of MCSF-R mRNA, which is similar to spleen DCs. In contrast, monocytes and microglia did not express Flt3 signal but did express high amounts of MCSF-R. GMCSF-R message was expressed by all cell populations, with higher levels noted in m/chDCs and CD8$^+$ spleen DCs (Fig. 4 A).

Looking further, we found that m/chDCs shared mRNA expression of many cell surface molecules with CD8$^+$ spleen DCs, including high CD103, CD24a, and CD36. They also expressed CD207 and CD205 mRNAs but at lower levels than CD8$^+$ DCs (Fig. 4 B). m/chDCs had high TLR3 and low TLR4 signals. TLR3 is a typical pattern recognition receptor on CD8$^+$ spleen DCs, whereas monocytes express high TLR4 and no TLR3 (Fig. 4 C). Similar to spleen DCs,

m/chDCs expressed high H2-DMb, H2-Aa, and H2-Ab, which are molecules critical for antigen presentation to $CD4^+$ T cells, but these were not expressed by monocytes or microglia. m/chDCs expressed intermediate levels of CD40 and CD80. To evaluate how the array data from Flt3L-expanded m/chDCs reflected those from the naive mice, we examined some of the cell surface markers in the naive mice with flow cytometry. Indeed, besides the aforementioned lineage markers CX_3CR1 (Fig. S2), Flt3, and CD115 (Fig. 3 A), phenotyping with CD11b, CD24, CD36, CD103, Dectin, EpCam, and CD205 confirmed the resemblance between m/chDCs and spleen DCs in untreated mice and the distinction from microglia (Fig. S4).

With respect to some other products, we noted that both spleen $CD8^+$ DCs and m/chDCs expressed high IL-12β mRNA, although IL-12α was not found (Fig. 4 D and not depicted). For transcription factors that program DC differentiation, m/chDCs demonstrated high expression of mRNAs for transcription factors Batf3, Id2, and RBP-J, each known to be involved in the differentiation of $CD8^+$ DCs in spleen (Fig. 4 E; Hacker et al., 2003; Caton et al., 2007; Hildner et al., 2008), suggesting a similar molecular programming during the development of m/chDCs and spleen DCs. Transcription factors differentially expressed in m/chDCs and spleen $CD8^+$ DCs include IRF-4, a transcription factor essential for $CD4^+$ splenic DC development (Fig. 4 E; Suzuki et al., 2004), suggesting tissue-specific differentiation programming. In summary, the gene expression profiles of m/chDCs suggest a close relationship with $CD8^+$ spleen DCs.

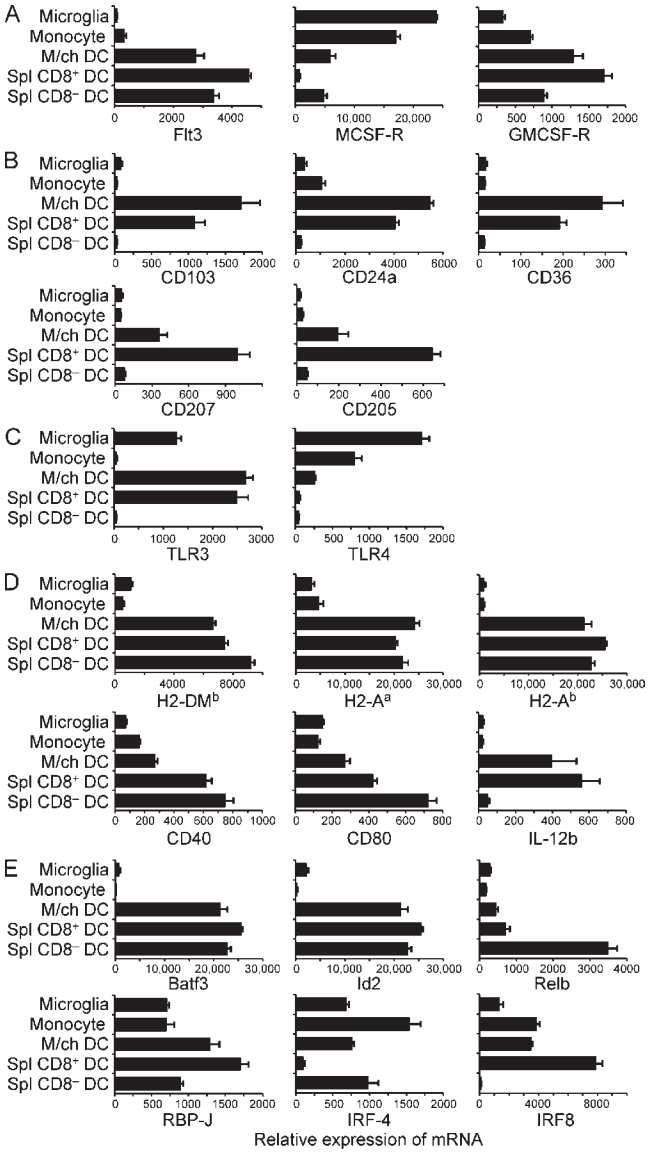

Figure 4. Gene expression profiles of m/chDC versus microglia, monocytes, and spleen DCs. Bone marrow monocytes, spleen (Spl) $CD8^+$ and $CD8^-$ DC subsets from untreated B6 mice and brain m/chDCs, and microglia from B6 mice treated with Flt3L were purified, and mRNA was extracted for Affymetrix gene array analysis. (A–E) Graphs show normalized data comparison among the indicated cells for expression of receptors for growth factors (A), cell surface markers (B), pattern recognition molecules (C), antigen presentation and co-stimulatory molecules (D), and transcription factors (E). Error bars indicate mean ± SEM ($n = 3$).

m/chDCs originate from a pre-DC marrow precursor and have a half-life of 5–7 d

To ascertain the origin of m/chDCs, we took advantage of our recent findings that the progenitors of lymphoid organ DCs and monocytes split during the transition between the monocyte and DC progenitor (MDP) and common DC progenitor (CDP) stages of development in the bone marrow (Fogg et al., 2006; Naik et al., 2007; Onai et al., 2007; Liu et al., 2009). Whereas MDPs give rise to monocytes and CDPs, the latter are restricted to produce DCs via migrating pre-DC intermediates. To examine whether DC precursors give rise to m/chDCs, we first adoptively transferred $Flt3^+$ BM DC precursors from CD11c-EYFP mice i.v. into non-irradiated naive mice. To examine the Flt3L responsiveness, we used $Flt3^{-/-}$ mice as recipient; thus, only donor cells could expand by Flt3L injection. 7 d after transfer, imaging of whole-mount brain indicated that donor-derived cells from $EYFP^+$ donor were only found in meninges but not parenchyma (Fig. S5). Furthermore, the donor cells were expanded by Flt3L injection (Fig. S5). To further investigate the exact precursor of the m/chDCs, we purified MDPs, CDPs, pre-DCs, and monocytes to >95% purity from the bone marrow and adoptively transferred them into the femurs of allotype-marked naive 3–4-wk-old mice. When we examined m/chDCs 1 wk later with flow cytometry, we found donor-derived brain DCs from mice that received 1–1.5 × 10^5 MDPs, CDPs, and pre-DCs (Fig. 5 A). In contrast, we did not detect any m/chDCs from mice that received 30–50 times more monocytes (5 × 10^6; Fig. 5 A). We reasoned that pre-DCs migrate to the brain meninges and choroids plexus where they further differentiate into cDCs, as we previously demonstrated in the spleen and lymph node (Liu et al., 2009). Indeed, a population of pre-DCs was detected in the brain leukocyte fraction and further enriched in meningeal preparation (0.3–0.4% of $CD45^+$ cells, which

is 10-fold higher than that of pre-DCs in blood; Fig. 5 B and Fig. S6). Similar to pre-DCs in spleen and blood, the brain pre-DCs were CX_3CR1-GFP^+ and expanded in situ in response to Flt3L injection (Fig. S6 C). Consistent with these adoptive transfer experiments, the exchange of m/chDCs in parabiotic mice was similar to blood pre-DCs and spleen DCs (Fig. 5 C), supporting a continuous equilibrium of m/chDCs with pre-DCs in the blood.

To measure the life span of m/chDCs, we tracked the decay of m/chDC chimerism in separated parabionts as we previously established (Liu et al., 2007; Ginhoux et al., 2009). Parabionts were established between CD45.1 and CD45.2 mice, and leukocytes were allowed to equilibrate in the tissues for >35 d before separation. In time course experiments, parabiont-derived m/chDCs showed a 50% decrease between 5 and 7 d and totally disappeared by day 14. Thus, m/chDCs have a half-life of 5–7 d, which is a similar life span to that of the spleen DCs (Fig. 5 D). We conclude that m/chDCs originate from pre-DCs and the DC developmental pathway in the bone marrow, and not from monocytes, and that they have a life span of ∼1–2 wk.

m/chDCs are effective in antigen presentation and stimulation of T cells

To examine antigen presentation in situ, the formation of peptide–MHC complexes by m/chDCs, we first stained cells with antibodies to the complex of I-Eα peptide on $I\text{-}A^b$ MHC II molecules (Y-Ae; Rudensky et al., 1991). Both spleen DCs and m/chDCs from BALB/c × B6 (CB1) mice stained positive for Y-Ae, whereas DCs from either BALB/c or C57BL/6 (B6) did not, indicating that DCs process and present an endogenous I-Eα peptide onto $I\text{-}A^b$ MHC II molecules (Fig. 6 A). In contrast, we did not detect this peptide–MHC complex on microglia from CB1 mice.

To evaluate the capacity of m/chDCs to initiate an immune response, we tested their ability to stimulate allogeneic T cells. Purified m/chDCs were compared with microglia and spleen DCs from Flt3L-injected B6 mice ($H\text{-}2^b$) by co-culture with CFSE-labeled bulk T cells ($H\text{-}2^d$) from BALB/c mice.

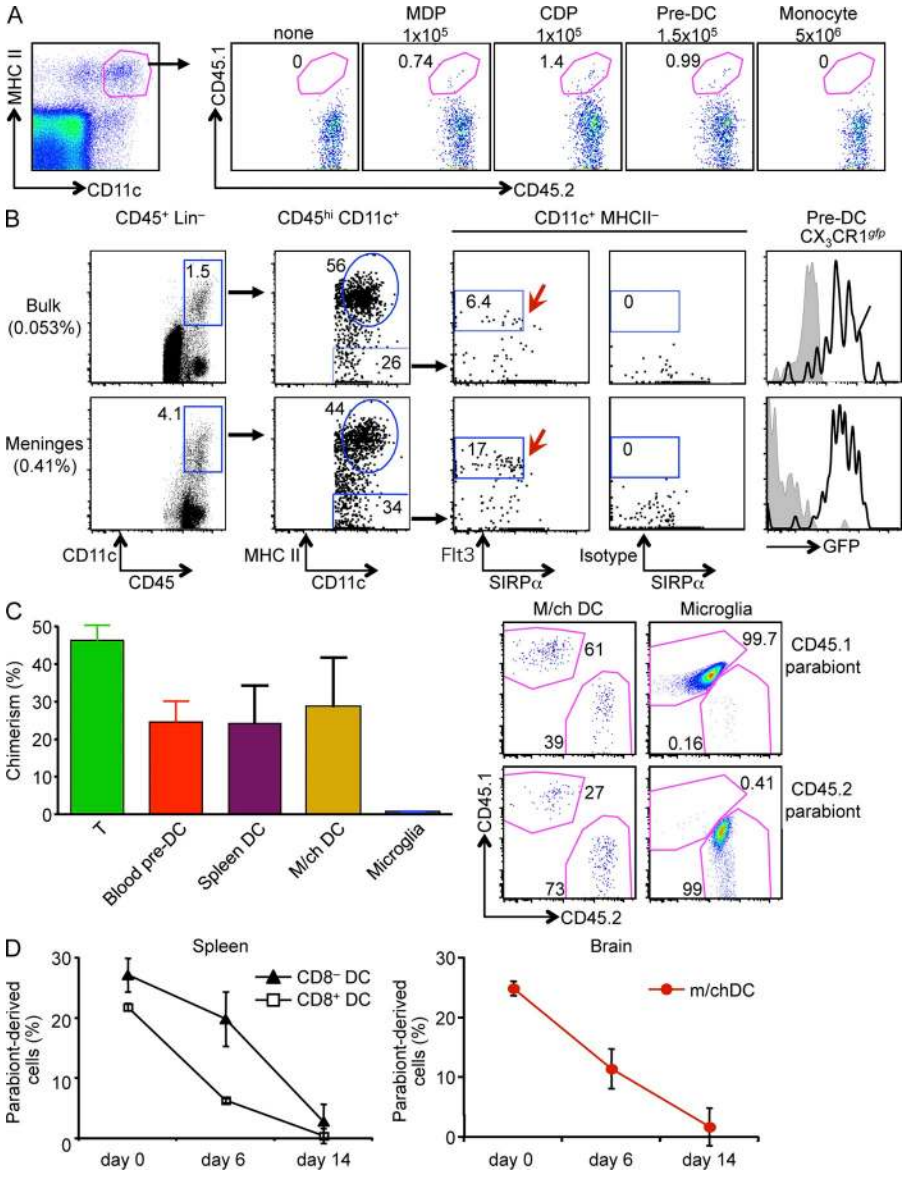

Figure 5. Origin and differentiation of brain m/chDCs. (A) The indicated numbers of purified MDPs, CDPs, pre-DCs, and monocytes from bone marrow of $CD45.1^+CD45.2^+$ mice were transferred into naive $CD45.2^+$ congenic hosts. Dot plots show the phenotype of m/chDCs, and the numbers indicate percentages derived from the donor 7 d after transfer. (B) Dot plots show percentages of $CD45^+Lin^-CD11c^+MHC\ II^-Flt3^+SIRP\alpha^{lo}$ pre-DCs among bulk brain and meningeal leukocytes. Numbers in the parentheses represent the mean pre-DC percentage of $CD45^+$ leukocytes (red arrows, pre-DCs). Histograms show GFP expression of gated pre-DCs in CX_3CR1^{gfp} (line) versus WT (shaded) mice. (C) CD45.1 and CD45.2 mice were surgically joined for 60 d. Graph shows the percentage of partner-derived T cells, blood pre-DCs, spleen DCs, brain m/chDCs, and microglia. Dot plots show representative percentages of CD45.1 and CD45.2 cells among m/chDCs and microglia in CD45.1 and CD45.2 parabionts. The bar graph shows two independent experiments with more than three mice in total. (D) CD45.2 and CD45.1 B6 mice were surgically joined for 60 d together before being separated. Graphs show the percentage of parabiont-derived DCs among each DC subset in the spleen and brain at different time points after separation. Bars represent two separate parabionts at each time point. (C and D) Error bars show mean ± SEM.

The m/chDCs and spleen DCs induced vigorous and comparable T cell proliferation, whereas microglia did not (Fig. 6 B).

To evaluate presentation of a self-antigen, myelin oligodendroglial glycoprotein (MOG) and MOG reactive, TCR transgenic T cells were used (Bettelli et al., 2003). Although the steady-state spleen DCs and m/chDCs did not present self-MOG antigen, they induced vigorous T cell proliferation when MOG peptide was added to the APC:T cell cultures, whereas microglia were inactive (Fig. 6 C). Therefore, although it has been reported that m/chDCs present self-antigen and stimulate T cell proliferation during the onset of neuroinflammation (Kivisäkk et al., 2009), in the steady-state, we did not observe priming of autoreactive T cells.

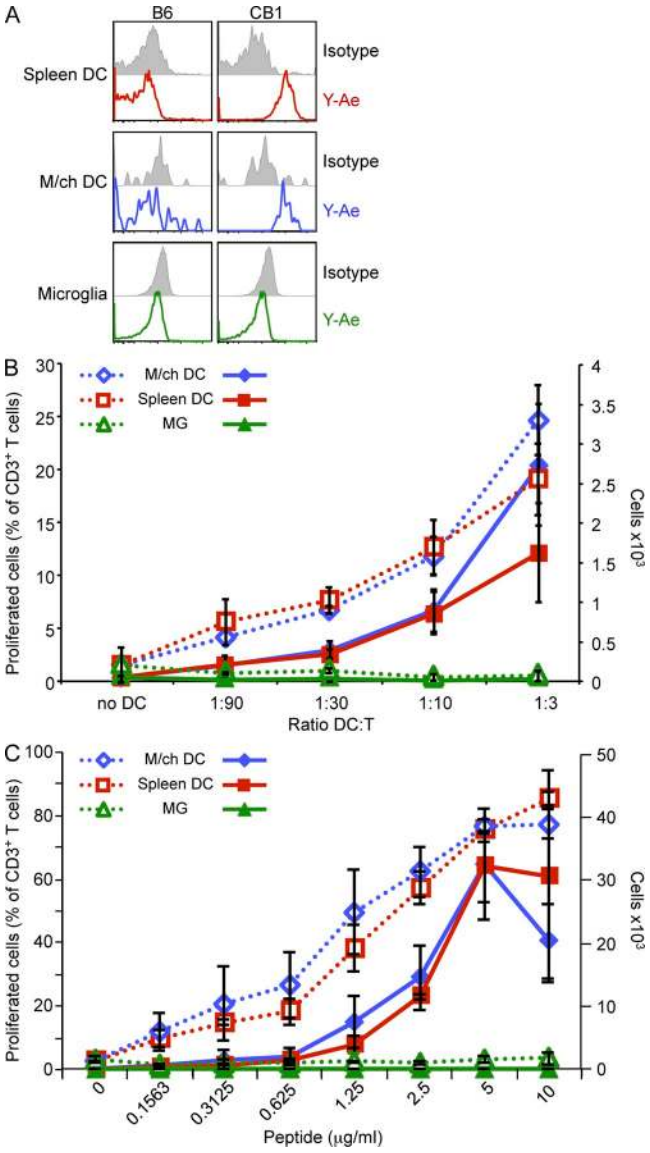

Figure 6. Antigen presentation by m/chDCs. (A) Flow cytometry histograms show Y-Ae antibody (line) or isotype (shaded area) staining of gated spleen DCs, brain m/chDCs, and microglia from B6 or BALB/c × B6 (CB1) mice. (B) CFSE-labeled BALB/c T cells were incubated with spleen DCs, brain m/chDCs, or microglia (MG) isolated from B6 mice treated with Flt3L and were analyzed with flow cytometry 4 d later. Graph shows percentage of proliferated T cells among total $CD3^+$ T cells, indicated by dilution of CFSE. One of three representative experiments is shown. (C) CFSE-labeled 2D2 MOG-specific $CD4^+$ transgenic T cells were incubated with spleen DCs, brain m/chDCs, or microglia isolated from B6 mice treated with Flt3L with the indicated doses of MOG peptide and were analyzed by flow cytometry 4 d later. Graph shows percentage of proliferated ($CFSE^{lo}$) T cells among total $CD3^+$ T cells. One of three representative experiments is shown. (B and C) Error bars show the SD between triplicate wells.

DISCUSSION

In this study, we demonstrate that $CD45^{hi}CD11c^{hi}$MHC II^{hi} cells in the meninges and choroid plexus of the steady-state mouse brain are typical DCs based on functional and developmental criteria. Our experiments on m/chDCs emphasize their resemblance to classical Flt3L-dependent DCs (cDCs) in spleen as well as major differences from microglia.

The entry of T cells into the parenchymal space is preceded by interaction with APCs in the leptomeningeal membrane, yet the nature and origin of these APCs were unclear. Using developmental and functional criteria, we observe CD11c and MHC II high stellate cells within the meninges and choroid plexus (m/chDCs) of naive mice and that these are authentic DCs in the steady-state brain positioned to meet and greet T cells along the avenues of effector T cell entry (Kivisäkk et al., 2003) and at the sites of IL-4 T cell recruitment during learning (Derecki et al., 2010). Although the m/chDCs are equipped with antigen-presenting machinery to interact with T cells, we did not observe T cell responses to autoreactive self-antigens in the healthy brain (Fig. 6 C). Yet when the balance is broken by neuroinflammation and self-antigen becomes readily available, these cells likely are able to present antigen to MOG-reactive T cells and accelerate the onset of disease (Kivisäkk et al., 2009; Wu et al., 2011). This is consistent with a previous study showing that Flt3L exacerbates disease severity in the experimental autoimmune encephalomyelitis model (Greter et al., 2005). Besides antigen presentation capacity, m/chDCs differ from parenchymal microglia in ontogeny. Ginhoux et al. (2010) demonstrated that the adult microglia arise from primitive myeloid progenitors before embryonic day 8 and do not need postnatal replenishment from blood. In contrast, like most cDCs in lymphoid tissues, m/chDCs have a 5–7-d half-life and as such are constantly replenished from bone marrow pre-DCs distinct from monocytes in an Flt3L-dependent manner. Our transcriptional profiling analysis further relates the m/chDCs to cDCs in spleen based on expression of transcription factors, including Batf3, RBP-J, and Id2, that are required for DC development. Functional analysis of purified m/chDCs indicates high surface levels of endogenous peptide–MHC complexes formed in situ, and when isolated they can actively stimulate alloreactive and MOG-reactive T cells in vitro. In all respects, m/chDCs differ from microglia, which are abundant in brain parenchyma.

Collectively, the unique anatomical distribution and antigen presentation features of m/chDCs support their role as an

educator at the gates during the onset of immune activity in the brain and help to explain the therapeutic effect of Flt3L inhibitor on reducing T cell infiltration in experimental autoimmune encephalomyelitis (Skarica et al., 2009). In the future, the targeted and specific ablation of m/chDCs in vivo will help to pinpoint their exact functions in brain meningeal immunity as well as cognitive process. The different ontogeny and function of m/chDCs and microglia have implications for immunotherapy of neurodegenerative and brain inflammatory diseases.

MATERIALS AND METHODS

Mice, parabiosis, and adoptive transfer. The CD11c-EYFP transgenic mouse was developed to identify DCs in vivo in the steady-state (Lindquist et al., 2004). *Flt3*$^{-/-}$ mice were generated and provided by I. Lemischka (Mount Sinai Medical Center, New York, NY), MHC II-EGFP knockin mice (Boes et al., 2002) were obtained from Taconic, and 2D2 MOG transgenic mice were obtained from The Jackson Laboratory. C57BL/6 and C57BL/6 Pep^{3b} CD45.1^{+} (SJL) mice were purchased from The Jackson Laboratory or were bred at the Rockefeller University.

Parabiotic mice were produced as described previously (Liu et al., 2007). Mice were anesthetized (2.5% [vol/vol] Avertin; Fluka) and shaved. Skin incisions were made in the sides of two adjacent mice from hip to elbow, and ligaments were sutured together with chromic gut (Ethicon); then the skin incisions were closed with 9-mm stainless-steel wound clips. Mice were kept on antibiotics for the 3 wk after surgery. For adoptive transfer, 5×10^5 or the indicated number of sorted purified progenitors or precursors were transferred i.v. For some experiments, recipient mice were conditioned with lethal irradiation, 550 cGy plus 500 cGy with 3 h between irradiations, and cell suspensions were injected i.v. immediately after the second irradiation. Mice were on antibiotic-supplemented food (TestDiet). All mice were maintained in specific pathogen–free conditions, and protocols were approved by the Rockefeller University Animal Care and Use Committee.

Reagents. The following reagents were from purchased from BD or eBioscience: anti-CD16-CD32 (2.4G2), biotin-conjugated anti–I-A/I-E (M5/114.15.2), anti–Y-Ae (eBioY-Ae), anti-CD45.2 (104), fluorescein isothiocyanate–conjugated anti-CD45.2 (104), phycoerythrin-conjugated anti-B220 (RA3-6B2), anti-CD40 (3/23), anti-CD62L (MEL-14), anti-CD24 (M1/69), anti-CD36 (no. 72-1), anti-CD103 (2E7), anti-CD115 (AFS98), anti-Flt3 (A2F10), phycoerythrin-indodicarbocyanine–conjugated anti-CD45.1 (A20), phycoerythrin–carbocyanine 5.5–conjugated anti–Gr-1(RB6-8C5), phycoerythrin-indotricarbocyanine–conjugated anti-CD3 (145-2C11), anti-CD19 (1D3), anti-NK1.1 (PK136), anti-Ter119 (TER-119), anti–Sca-1 (D7), anti-CD11b (M1/70), anti-CD11c (N418), anti–Gr-1 (RB6-8C5), anti-B220 (RA3-6B2), Pacific blue–conjugated anti-CD11b (M1/70), anti-B220 (RA3-6B2), allophycocyanin-conjugated anti-CD11b (M1/70), anti-CD11c (N418), anti-SIRPα (P84), anti-CD205 (205yekta), anti-F4/80 (BM8), anti–Dectin-1 (2A11; from AbD Serotec), anti–c-Kit (2B8), Alexa Fluor 700–conjugated anti–I-A/I-E (M5/114.15.2), Alexa Fluor 750–conjugated anti-CD11b (M1/70), anti-CD11c (N418), BD Lyse lysing buffer, Cytoperm/Cytofix solution, and Perm/Wash buffer. DAPI was purchased from Invitrogen. Antibiotin and anti-CD11c microbeads were obtained from Miltenyi Biotec. Other reagents used included PBS, FBS, and ACK lysing buffer (all Invitrogen).

Cell preparation. 6–8-wk-old C57BL/6 F mice were injected s.c. to the flank with 5×10^6 B16 murine Flt3L-secreting tumor cells. Between 12 and 16 d at ∼8-mm tumor size, mice were sacrificed, and intracardiac perfusion was performed on Flt3L-treated and control mice using PBS with heparin (1 USP unit/ml) with observed blanching of the spleen. Brains with meninges and spleen were dissected. For some experiments, meninges were carefully removed with fine tweezers. Brain tissue was finely minced into confetti-sized pieces and treated with 375 mU/ml collagenase (type II; Roche) with 400 mg DNase in Hanks' buffer for 45 min at 37°C, followed by homogenization with vigorous pipetting using glass pipettes. Homogenates were reincubated for 15 min at 37°C. 20 mM EDTA was added for 5 min at 37°C. All subsequent washes were performed with ice-cold PBS with 2% FCS. Brain homogenate was washed and filtered once through a 100-μM filter to remove undigested fragments and then washed twice again, followed by centrifugation at 2,000 rpm for 10 min. Cells were resuspended in 40% Percoll under 5 ml PBS and centrifuged at 1,200 *g* for 25 min (slow accelerations and decelerations off) at 20°C in a J-20 rotor (Sorvall). Cells were harvested from the pellet, washed twice, and incubated in Fc block with 2% rat serum before cell surface marker antibody staining. Spleens and meninges were mixed in 5 ml Hanks' buffer containing 375 mU/ml collagenase (type II), teased apart, and then incubated for 25 min at 37°C. For disruption of DC–T cell complexes, 10 mM EDTA was added, and mixing continued for the last 5 min of incubation. For spleen cell preparation, ACK lysis of red blood cells was followed by washing twice and filtering undigested fibrous material through a 100-mm cell strainer. All subsequent steps were performed at 4°C with 5% (vol/vol) FBS in PBS. Undigested fibrous material was removed by filtration through a 100-mm cell strainer. All subsequent steps were performed at 4°C with 5% (vol/vol) FBS in PBS.

For adoptive transfer experiments, MDPs, CDPs, and pre-cDCs were pre-enriched by biotin–anti-Flt3 antibody followed by antibiotin microbeads. Monocytes were pre-enriched by biotin–anti-CD115 antibody followed by antibiotin microbeads. Positive fractions from Miltenyi Biotec columns were eluted and either directly used to transfer or stained and sorted on FACS Aria (BD) to >95% purity.

Antigen presentation assays. For the mixed leukocyte reaction, T cells were enriched by negative selection from BALB/c and B6 spleen and lymph nodes by grinding organs between two frosted glass slides into complete RPMI medium with 5% FCS. Cells were washed twice, followed by filtration of debris through a 70-μM filter, and then incubated in MACS buffer (2% FCS and 2 mM EDTA) with biotin-labeled CD11b, B220, DX5 (CD49b), Gr.1, MHC II (I-A/I-E), and Ter119 antibodies. Subsequent streptavidin bead incubation and negative enrichment were performed via the MACS (Miltenyi Biotec) LD column as per the manufacturer's instructions. Flow through was collected. T cells were counted and resuspended in 10^7 cells/ml PBS with the addition of 1 nM CFSE and incubated at 37° for 10 min and then washed twice in complete RPMI medium with 5% FCS. 5×10^4 CFSE-labeled T cells were plated per well with titrated ratios of m/chDC, spleen DC, and microglia populations after sort. At day 4, samples were stained with live/dead AQUA, Thy1.2, CD3, CD4, and CD8 antibodies and gated on CFSE divisions in CD3^{+}Thy1.2^{+}CD4/8^{+} subsets. To directly detect a self-antigen–MHC complex, we used Y-Ae mAb to identify complexes of I-Eα peptide presented on I-A^{b} molecules in BALB/c × C57BL/6 (CB1) mice, with BALB/c (I-Eα only) and C57BL/6 (I-A^{b} only) serving as controls.

For presentation of a myelin peptide to T cells, we used MOG 2D2 transgenic CD4^{+} T cells negatively enriched by MACS sorting from lymph nodes (mesenteric and skin draining) and spleens. 5×10^4 CFSE-labeled T cells per well were cultured with a maximum of 10 mg/ml MOG peptide (33–55) MEVGWYRSPFSRVVHLYRNGK at 99% purity (American Peptide Company). DC populations were co-cultured with T cells at a ratio of 1:10 DC/T cells.

Flow cytometry and sorting. Cells were stained on ice in PBS with 2.0% (vol/vol) FCS. LSR II (BD) was used for multiparameter flow cytometry of stained cell suspensions, followed by analysis with FlowJo software (Tree Star). Cells were gated as follows: microglia, Lin^{-} (CD19^{-}CD3^{-}NK1.1^{-}B220^{-}Ter119^{-}) CD45^{int}CD11c^{-}; DCs, Lin^{-}CD45^{hi}CD11c^{+}; polymorphonuclear leukocytes, CD3^{-}CD19^{-}NK1.1^{-}Ter119^{-}SSC^{hi}CD11b^{hi}Gr-1^{hi}; monocytes, SSC^{lo}CD11b^{hi}CD115^{+}; CD8^{+} spleen DCs, Lin^{-} (CD19^{-}CD3^{-}NK1.1^{-}B220^{-}Ter119^{-}) CD11c^{+}CD8^{+}; and CD8^{-} spleen DCs, Lin^{-} (CD19^{-}CD3^{-}NK1.1^{-}B220^{-}Ter119^{-}) CD11c^{+}CD8^{-}. Dead cells were excluded with DAPI or AQUA staining.

Microarray. Microglia and brain DCs from brain, monocytes from bone marrow, and $CD8^+$ and $CD8^-$ cDCs from spleen were purified by sorting from WT mice or mice injected with Flt3L-producing B16 melanoma cells. All cell samples were purified to >98% homogeneity. Total RNA extraction and DNA microarray analysis of gene expression were performed at the gene array facility (Memorial Sloan-Kettering Cancer Center, New York, NY). Fluorescent images of hybridized microarrays (MOE-430 2.0; Affymetrix) were obtained using a Genechip scanner (Affymetrix). Microarray data were analyzed using GeneSpring 10.0 software (Affymetrix). All samples were repeated at least three times with individually sorted cells and averaged. Microarray data are available in the National Center for Biotechnology Information GEO DataSets under accession no. GSE29949.

Two-photon microscopy. In some experiments, cardiac perfusion was performed using PBS and 4% paraformaldehyde, and intact whole brains with meninges were embedded in low molecular weight agarose. Brains were cut into 4–5-mm coronal sections to access the ventricles for imaging of the choroid plexus. To image meninges, the brains were removed from the mouse and positioned up-right in a 30-mm Petri dish containing PBS and covered with a coverslip. To image the choroid plexus, brains coronally at the midcortex were positioned in the Petri dish with the surgical margin facing upward and covered with a coverslip. Images of meninges and choroid plexus with surrounding parenchyma were obtained using a multiphoton laser-scanning microscope (Fluoview FV 1000MPE; Olympus) fitted with a Coherent Chameleon Vision II laser (tunable from 690–1,040 nm) and a 25×/NA 1.05 objective, controlled by FluoView (FV-10) software (Olympus) at the Rockefeller University Bio-Imaging Facility. To image EGFP and EYFP, the excitation wavelength was set between 910 and 930 nm; emission light was split by two dichroic mirrors at 510 and 560 nm into three channels, and band-pass filters optimized for detecting second harmonics (dichroic 510 nm, hq 460–510), EYFP (hq 495–540), and dsRed (hq 570–625) were used for detection.

In some experiments, blood vessels were directly labeled by cardiac perfusion using a specially formulated aqueous solution containing 1,1′-dioctadecyl-3,3,3′,3′-tetramethylindocarbocyanine perchlorate (DiI; Sigma-Aldrich) as previously described (Li et al., 2008). In brief, mice were perfused sequentially with PBS, DiI, and 4% paraformaldehyde. To visualize the meninges and choroid plexus in depth, tiled z stacks (300-mm deep and 10-µm z resolution) were acquired. Volocity (PerkinElmer) and Imaris (Bitplane) software were used for data representation. Photoshop (Adobe) was used for final processing.

Online supplemental material. Fig. S1 shows $CD11c^+MHC\ II^+$ cDCs in the spleen, bulk brain, and meninges. Fig. S2 shows CX_3CR1 expression on m/chDCs. Fig. S3 shows that Flt3L treatment does not induce DC maturation. Fig. S4 shows the phenotype of m/chDCs. Fig. S5 shows that DC precursors populate meninges. Fig. S6 shows pre-DCs in the meninges and their expansion induced by Flt3L. Video 1 shows the distribution of EGFP cells in the meninges and parenchyma in the brain of $I\text{-}A^b$ mice. Online supplemental material is available at http://www.jem.org/cgi/content/full/jem.20102657/DC1.

We would like to thank Judy Adams for expertise in figures, Dr. Juliana Idoyaga for providing $Flt3^{-/-}$ CD45.1 mice, personnel in the Rockefeller University Comparative Bioscience Center, Flow Cytometry Resource Center, and the Bio-Imaging Resource Center for expert technical assistance, and Dr. Karen Bulloch for valuable discussions.

This research is supported in part by a gift from the Peter Deane Trust and grants from the National Institutes of Health (AI13013 to R.M. Steinman) and the Dana Foundation (to K. Liu, M.L. Dustin, and R.M. Steinman). M.C. Nussenzweig was supported by the Howard Hughes Medical Institute. N. Anandasabapathy was supported in part by a Sulzberger Fellowship from the Ronald O. Perelman Department of Dermatology at the New York University School of Medicine and the Rockefeller University Clinical and Translation Science Award. Support for the Rockefeller University Flow Cytometry Facility and multiphoton microscope was provided by the Empire State Stem Cell fund through New York State Department of Health (NYSDOH) contract #C023046. Opinions expressed here are solely those of the authors and do not necessarily reflect those of the Empire State Stem Cell Fund, the NYSDOH, or the State of New York.

The authors have no further conflicting financial interests.

Submitted: 22 December 2010
Accepted: 28 June 2011

REFERENCES

Axtell, R.C., and L. Steinman. 2009. Gaining entry to an uninflamed brain. *Nat. Immunol.* 10:453–455. doi:10.1038/ni0509-453

Bailey, S.L., P.A. Carpentier, E.J. McMahon, W.S. Begolka, and S.D. Miller. 2006. Innate and adaptive immune responses of the central nervous system. *Crit. Rev. Immunol.* 26:149–188.

Bailey, S.L., B. Schreiner, E.J. McMahon, and S.D. Miller. 2007. CNS myeloid DCs presenting endogenous myelin peptides 'preferentially' polarize CD4+ T(H)-17 cells in relapsing EAE. *Nat. Immunol.* 8:172–180. doi:10.1038/ni1430

Banchereau, J., and R.M. Steinman. 1998. Dendritic cells and the control of immunity. *Nature.* 392:245–252. doi:10.1038/32588

Bartholomäus, I., N. Kawakami, F. Odoardi, C. Schläger, D. Miljkovic, J.W. Ellwart, W.E. Klinkert, C. Flügel-Koch, T.B. Issekutz, H. Wekerle, and A. Flügel. 2009. Effector T cell interactions with meningeal vascular structures in nascent autoimmune CNS lesions. *Nature.* 462:94–98. doi:10.1038/nature08478

Bettelli, E., M. Pagany, H.L. Weiner, C. Linington, R.A. Sobel, and V.K. Kuchroo. 2003. Myelin oligodendrocyte glycoprotein–specific T cell receptor transgenic mice develop spontaneous autoimmune optic neuritis. *J. Exp. Med.* 197:1073–1081. doi:10.1084/jem.20021603

Boes, M., J. Cerny, R. Massol, M. Op den Brouw, T. Kirchhausen, J. Chen, and H.L. Ploegh. 2002. T-cell engagement of dendritic cells rapidly rearranges MHC class II transport. *Nature.* 418:983–988. doi:10.1038/nature01004

Bogunovic, M., F. Ginhoux, J. Helft, L. Shang, D. Hashimoto, M. Greter, K. Liu, C. Jakubzick, M.A. Ingersoll, M. Leboeuf, et al. 2009. Origin of the lamina propria dendritic cell network. *Immunity.* 31:513–525. doi:10.1016/j.immuni.2009.08.010

Caton, M.L., M.R. Smith-Raska, and B. Reizis. 2007. Notch–RBP-J signaling controls the homeostasis of $CD8^-$ dendritic cells in the spleen. *J. Exp. Med.* 204:1653–1664. doi:10.1084/jem.20062648

Choi, J.H., Y. Do, C. Cheong, H. Koh, S.B. Boscardin, Y.S. Oh, L. Bozzacco, C. Trumpfheller, C.G. Park, and R.M. Steinman. 2009. Identification of antigen-presenting dendritic cells in mouse aorta and cardiac valves. *J. Exp. Med.* 206:497–505. doi:10.1084/jem.20082129

Derecki, N.C., A.N. Cardani, C.H. Yang, K.M. Quinnies, A. Crihfield, K.R. Lynch, and J. Kipnis. 2010. Regulation of learning and memory by meningeal immunity: a key role for IL-4. *J. Exp. Med.* 207:1067–1080. doi:10.1084/jem.20091419

Dudziak, D., A.O. Kamphorst, G.F. Heidkamp, V.R. Buchholz, C. Trumpfheller, S. Yamazaki, C. Cheong, K. Liu, H.W. Lee, C.G. Park, et al. 2007. Differential antigen processing by dendritic cell subsets in vivo. *Science.* 315:107–111. doi:10.1126/science.1136080

Fogg, D.K., C. Sibon, C. Miled, S. Jung, P. Aucouturier, D.R. Littman, A. Cumano, and F. Geissmann. 2006. A clonogenic bone marrow progenitor specific for macrophages and dendritic cells. *Science.* 311:83–87. doi:10.1126/science.1117729

Geissmann, F., S. Jung, and D.R. Littman. 2003. Blood monocytes consist of two principal subsets with distinct migratory properties. *Immunity.* 19:71–82. doi:10.1016/S1074-7613(03)00174-2

Geissmann, F., S. Gordon, D.A. Hume, A.M. Mowat, and G.J. Randolph. 2010. Unravelling mononuclear phagocyte heterogeneity. *Nat. Rev. Immunol.* 10:453–460. doi:10.1038/nri2784

Ginhoux, F., K. Liu, J. Helft, M. Bogunovic, M. Greter, D. Hashimoto, J. Price, N. Yin, J. Bromberg, S.A. Lira, et al. 2009. The origin and development of nonlymphoid tissue $CD103^+$ DCs. *J. Exp. Med.* 206:3115–3130. doi:10.1084/jem.20091756

Ginhoux, F., M. Greter, M. Leboeuf, S. Nandi, P. See, S. Gokhan, M.F. Mehler, S.J. Conway, L.G. Ng, E.R. Stanley, et al. 2010. Fate mapping analysis reveals that adult microglia derive from primitive macrophages. *Science.* 330:841–845. doi:10.1126/science.1194637

Gottfried-Blackmore, A., U.W. Kaunzner, J. Idoyaga, J.C. Felger, B.S. McEwen, and K. Bulloch. 2009. Acute in vivo exposure to interferon-gamma enables resident brain dendritic cells to become effective antigen presenting cells. *Proc. Natl. Acad. Sci. USA.* 106:20918–20923. doi:10.1073/pnas.0911509106

Greter, M., F.L. Heppner, M.P. Lemos, B.M. Odermatt, N. Goebels, T. Laufer, R.J. Noelle, and B. Becher. 2005. Dendritic cells permit immune invasion of the CNS in an animal model of multiple sclerosis. *Nat. Med.* 11:328–334. doi:10.1038/nm1197

Hacker, C., R.D. Kirsch, X.S. Ju, T. Hieronymus, T.C. Gust, C. Kuhl, T. Jorgas, S.M. Kurz, S. Rose-John, Y. Yokota, and M. Zenke. 2003. Transcriptional profiling identifies Id2 function in dendritic cell development. *Nat. Immunol.* 4:380–386. doi:10.1038/ni903

Heath, W.R., and F.R. Carbone. 2009. Dendritic cell subsets in primary and secondary T cell responses at body surfaces. *Nat. Immunol.* 10:1237–1244. doi:10.1038/ni.1822

Henri, S., M. Guilliams, L.F. Poulin, S. Tamoutounour, L. Ardouin, M. Dalod, and B. Malissen. 2010. Disentangling the complexity of the skin dendritic cell network. *Immunol. Cell Biol.* 88:366–375. doi:10.1038/icb.2010.34

Hess, L.M., and K.C. Insel. 2007. Chemotherapy-related change in cognitive function: a conceptual model. *Oncol. Nurs. Forum.* 34:981–994. doi:10.1188/07.ONF.981-994

Hickey, W.F. 1991. Migration of hematogenous cells through the blood-brain barrier and the initiation of CNS inflammation. *Brain Pathol.* 1:97–105. doi:10.1111/j.1750-3639.1991.tb00646.x

Hildner, K., B.T. Edelson, W.E. Purtha, M. Diamond, H. Matsushita, M. Kohyama, B. Calderon, B.U. Schraml, E.R. Unanue, M.S. Diamond, et al. 2008. Batf3 deficiency reveals a critical role for CD8alpha+ dendritic cells in cytotoxic T cell immunity. *Science.* 322:1097–1100. doi:10.1126/science.1164206

Jung, S., D. Unutmaz, P. Wong, G. Sano, K. De los Santos, T. Sparwasser, S. Wu, S. Vuthoori, K. Ko, F. Zavala, et al. 2002. In vivo depletion of CD11c+ dendritic cells abrogates priming of CD8+ T cells by exogenous cell-associated antigens. *Immunity.* 17:211–220. doi:10.1016/S1074-7613(02)00365-5

Kingston, D., M.A. Schmid, N. Onai, A. Obata-Onai, D. Baumjohann, and M.G. Manz. 2009. The concerted action of GM-CSF and Flt3-ligand on in vivo dendritic cell homeostasis. *Blood.* 114:835–843. doi:10.1182/blood-2009-02-206318

Kipnis, J., N.C. Derecki, C. Yang, and H. Scrable. 2008. Immunity and cognition: what do age-related dementia, HIV-dementia and 'chemo-brain' have in common? *Trends Immunol.* 29:455–463. doi:10.1016/j.it.2008.07.007

Kivisäkk, P., D.J. Mahad, M.K. Callahan, C. Trebst, B. Tucky, T. Wei, L. Wu, E.S. Baekkevold, H. Lassmann, S.M. Staugaitis, et al. 2003. Human cerebrospinal fluid central memory CD4+ T cells: evidence for trafficking through choroid plexus and meninges via P-selectin. *Proc. Natl. Acad. Sci. USA.* 100:8389–8394. doi:10.1073/pnas.1433000100

Kivisäkk, P., J. Imitola, S. Rasmussen, W. Elyaman, B. Zhu, R.M. Ransohoff, and S.J. Khoury. 2009. Localizing central nervous system immune surveillance: meningeal antigen-presenting cells activate T cells during experimental autoimmune encephalomyelitis. *Ann. Neurol.* 65:457–469. doi:10.1002/ana.21379

Lemos, M.P., L. Fan, D. Lo, and T.M. Laufer. 2003. CD8alpha+ and CD11b+ dendritic cell-restricted MHC class II controls Th1 CD4+ T cell immunity. *J. Immunol.* 171:5077–5084.

Li, Y., Y. Song, L. Zhao, G. Gaidosh, A.M. Laties, and R. Wen. 2008. Direct labeling and visualization of blood vessels with lipophilic carbocyanine dye DiI. *Nat. Protoc.* 3:1703–1708. doi:10.1038/nprot.2008.172

Lindquist, R.L., G. Shakhar, D. Dudziak, H. Wardemann, T. Eisenreich, M.L. Dustin, and M.C. Nussenzweig. 2004. Visualizing dendritic cell networks in vivo. *Nat. Immunol.* 5:1243–1250. doi:10.1038/ni1139

Liu, K., C. Waskow, X. Liu, K. Yao, J. Hoh, and M. Nussenzweig. 2007. Origin of dendritic cells in peripheral lymphoid organs of mice. *Nat. Immunol.* 8:578–583. doi:10.1038/ni1462

Liu, K., G.D. Victora, T.A. Schwickert, P. Guermonprez, M.M. Meredith, K. Yao, F.F. Chu, G.J. Randolph, A.Y. Rudensky, and M. Nussenzweig. 2009. In vivo analysis of dendritic cell development and homeostasis. *Science.* 324:392–397. doi:10.1126/science.1170540

Matyszak, M.K., and V.H. Perry. 1996. The potential role of dendritic cells in immune-mediated inflammatory diseases in the central nervous system. *Neuroscience.* 74:599–608. doi:10.1016/0306-4522(96)00160-1

McMenamin, P.G. 1999. Distribution and phenotype of dendritic cells and resident tissue macrophages in the dura mater, leptomeninges, and choroid plexus of the rat brain as demonstrated in wholemount preparations. *J. Comp. Neurol.* 405:553–562. doi:10.1002/(SICI)1096-9861(19990322)405:4<553::AID-CNE8>3.0.CO;2-6

McMenamin, P.G., R.J. Wealthall, M. Deverall, S.J. Cooper, and B. Griffin. 2003. Macrophages and dendritic cells in the rat meninges and choroid plexus: three-dimensional localisation by environmental scanning electron microscopy and confocal microscopy. *Cell Tissue Res.* 313:259–269. doi:10.1007/s00441-003-0779-0

Mildner, A., H. Schmidt, M. Nitsche, D. Merkler, U.K. Hanisch, M. Mack, M. Heikenwalder, W. Brück, J. Priller, and M. Prinz. 2007. Microglia in the adult brain arise from Ly-6ChiCCR2+ monocytes only under defined host conditions. *Nat. Neurosci.* 10:1544–1553. doi:10.1038/nn2015

Naik, S.H., P. Sathe, H.Y. Park, D. Metcalf, A.I. Proietto, A. Dakic, S. Carotta, M. O'Keeffe, M. Bahlo, A. Papenfuss, et al. 2007. Development of plasmacytoid and conventional dendritic cell subtypes from single precursor cells derived in vitro and in vivo. *Nat. Immunol.* 8:1217–1226. doi:10.1038/ni1522

Onai, N., A. Obata-Onai, M.A. Schmid, T. Ohteki, D. Jarrossay, and M.G. Manz. 2007. Identification of clonogenic common Flt3+M-CSFR+ plasmacytoid and conventional dendritic cell progenitors in mouse bone marrow. *Nat. Immunol.* 8:1207–1216. doi:10.1038/ni1518

Platten, M., and L. Steinman. 2005. Multiple sclerosis: trapped in deadly glue. *Nat. Med.* 11:252–253. doi:10.1038/nm0305-252

Price, R.W., B. Brew, J. Sidtis, M. Rosenblum, A.C. Scheck, and P. Cleary. 1988. The brain in AIDS: central nervous system HIV-1 infection and AIDS dementia complex. *Science.* 239:586–592. doi:10.1126/science.3277272

Reboldi, A., C. Coisne, D. Baumjohann, F. Benvenuto, D. Bottinelli, S. Lira, A. Uccelli, A. Lanzavecchia, B. Engelhardt, and F. Sallusto. 2009. C-C chemokine receptor 6-regulated entry of TH-17 cells into the CNS through the choroid plexus is required for the initiation of EAE. *Nat. Immunol.* 10:514–523. doi:10.1038/ni.1716

Rescigno, M., and A. Di Sabatino. 2009. Dendritic cells in intestinal homeostasis and disease. *J. Clin. Invest.* 119:2441–2450. doi:10.1172/JCI39134

Rudensky, A.Yu., S. Rath, P. Preston-Hurlburt, D.B. Murphy, and C.A. Janeway Jr. 1991. On the complexity of self. *Nature.* 353:660–662. doi:10.1038/353660a0

Serafini, B., B. Rosicarelli, R. Magliozzi, E. Stigliano, E. Capello, G.L. Mancardi, and F. Aloisi. 2006. Dendritic cells in multiple sclerosis lesions: maturation stage, myelin uptake, and interaction with proliferating T cells. *J. Neuropathol. Exp. Neurol.* 65:124–141. doi:10.1097/01.jnen.0000199572.96472.1c

Skarica, M., T. Wang, E. McCadden, D. Kardian, P.A. Calabresi, D. Small, and K.A. Whartenby. 2009. Signal transduction inhibition of APCs diminishes th17 and Th1 responses in experimental autoimmune encephalomyelitis. *J. Immunol.* 182:4192–4199. doi:10.4049/jimmunol.0803631

Suzuki, S., K. Honma, T. Matsuyama, K. Suzuki, K. Toriyama, I. Akitoyo, K. Yamamoto, T. Suematsu, M. Nakamura, K. Yui, and A. Kumatori. 2004. Critical roles of interferon regulatory factor 4 in CD11bhighCD8alpha-dendritic cell development. *Proc. Natl. Acad. Sci. USA.* 101:8981–8986. doi:10.1073/pnas.0402139101

Varol, C., A. Vallon-Eberhard, E. Elinav, T. Aychek, Y. Shapira, H. Luche, H.J. Fehling, W.D. Hardt, G. Shakhar, and S. Jung. 2009. Intestinal lamina propria dendritic cell subsets have different origin and functions. *Immunity.* 31:502–512. doi:10.1016/j.immuni.2009.06.025

Waskow, C., K. Liu, G. Darrasse-Jèze, P. Guermonprez, F. Ginhoux, M. Merad, T. Shengelia, K. Yao, and M. Nussenzweig. 2008. The receptor tyrosine kinase Flt3 is required for dendritic cell development in peripheral lymphoid tissues. *Nat. Immunol.* 9:676–683. doi:10.1038/ni.1615

Wolf, S.A., B. Steiner, A. Akpinarli, T. Kammertoens, C. Nassenstein, A. Braun, T. Blankenstein, and G. Kempermann. 2009. CD4-positive T lymphocytes provide a neuroimmunological link in the control of adult hippocampal neurogenesis. *J. Immunol.* 182:3979–3984. doi:10.4049/jimmunol.0801218

Wu, G.F., K.S. Shindler, E.J. Allenspach, T.L. Stephen, H.L. Thomas, R.J. Mikesell, A.H. Cross, and T.M. Laufer. 2011. Limited sufficiency of antigen presentation by dendritic cells in models of central nervous system autoimmunity. *J. Autoimmun.* 36:56–64. doi:10.1016/j.jaut.2010.10.006

Ziv, Y., N. Ron, O. Butovsky, G. Landa, E. Sudai, N. Greenberg, H. Cohen, J. Kipnis, and M. Schwartz. 2006. Immune cells contribute to the maintenance of neurogenesis and spatial learning abilities in adulthood. *Nat. Neurosci.* 9:268–275. doi:10.1038/nn1629